Acta Pharmaceutica Sinica B 2020;10(6):1047−1060

Chinese Pharmaceutical Association
Institute of Materia Medica, Chinese Academy of Medical Sciences

Acta Pharmaceutica Sinica B

www.elsevier.com/locate/apsb
www.sciencedirect.com

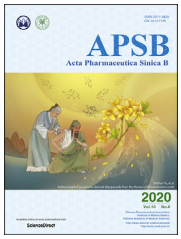

ORIGINAL ARTICLE

A novel cyclic peptide targeting LAG-3 for cancer immunotherapy by activating antigen-specific CD8$^+$ T cell responses

Wenjie Zhai[a], Xiuman Zhou[a], Hongfei Wang[a], Wanqiong Li[b], Guanyu Chen[b], Xinghua Sui[b], Guodong Li[a], Yuanming Qi[a,*], Yanfeng Gao[a,b,*]

[a]*School of Life Sciences, Zhengzhou University, Zhengzhou 450001, China*
[b]*School of Pharmaceutical Sciences (Shenzhen), Sun Yat-sen University, Guangzhou 510006, China*

Received 29 June 2019; received in revised form 10 October 2019; accepted 26 November 2019

KEY WORDS

LAG-3;
Phage display;
Cyclic peptide;
Immune checkpoint blockade;
CD8$^+$ T cell;
Cancer immunotherapy

Abstract PD-1 and CTLA-4 antibodies offer great hope for cancer immunotherapy. However, many patients are incapable of responding to PD-1 and CTLA-4 blockade and show low response rates due to insufficient immune activation. The combination of checkpoint blockers has been proposed to increase the response rates. Besides, antibody drugs have disadvantages such as inclined to cause immune-related adverse events and infiltration problems. In this study, we developed a cyclic peptide C25 by using Ph.D.-C7C phage display technology targeting LAG-3. As a result, C25 showed a relative high affinity with human LAG-3 protein and could effectively interfere the binding between LAG-3 and HLA-DR (MHC-II). Additionally, C25 could significantly stimulate CD8$^+$ T cell activation in human PBMCs. The results also demonstrated that C25 could inhibit tumor growth of CT26, B16 and B16-OVA bearing mice, and the infiltration of CD8$^+$ T cells was significantly increased while FOXP3$^+$ Tregs significantly decreased in the tumor site. Furthermore, the secretion of IFN-γ by CD8$^+$ T cells in spleen, draining lymph nodes and especially in the tumors was promoted. Simultaneously, we exploited T cells depletion models to study the anti-tumor mechanisms for C25 peptide, and the results combined with MTT assay confirmed that C25 exerted anti-tumor effects *via* CD8$^+$ T cells but not direct killing. In conclusion, cyclic peptide C25 provides a rationale for targeting the immune checkpoint, by blockade of LAG-3/HLA-DR interaction in order to enhance

*Corresponding authors. Tel.: +86 20 84723750.
E-mail addresses: qym@zzu.edu.cn (Yuanming Qi), gaoyf29@mail.sysu.edu.cn (Yanfeng Gao).
Peer review under responsibility of Institute of Materia Medica, Chinese Academy of Medical Sciences and Chinese Pharmaceutical Association.

https://doi.org/10.1016/j.apsb.2020.01.005

anti-tumor immunity, and C25 may provide an alternative for cancer immunotherapy besides antibody drugs.

1. Introduction

Immune checkpoint blockade that activates body immunity for anti-tumor therapy has achieved great success[1,2], especially by targeting cytotoxic T cell antigen 4 (CTLA-4, CD152) and programmed death 1 (PD-1, CD279)/PD-L1 (programmed cell death ligand 1, CD274, the ligand of PD-1). Until now, at least seven CTLA-4 or PD-1/PD-L1 antibody drugs have been approved by the U.S. Food and Drug Administration (FDA) for the treatment of different types of cancer, including one CTLA-4 (ipilimumab), three PD-1 antibodies (nivolumab, pembrolizumab and cemiplimab) and three PD-L1 antibodies (atezolizumab, avelumab and durvalumab). These antibodies have been used to treat patients with melanoma, lung cancer, head and neck cancers, bladder cancer, Merkel cell carcinoma and classic Hodgkin's lymphoma, etc[3−9]. However, a large number of patients with solid tumors showed resistance to the anti-PD-1 and anti-CTLA-4 therapy[10]. Such as colorectal cancer, only a small percentage of patients are able to respond to single immune checkpoint[3,11]. It is reported that various immune checkpoints are up-regulated on exhausted T cells in the tumor microenvironment (TME), such as T-cell immunoglobulin and mucin containing protein-3 (TIM-3, CD366), T-cell immunoglobulin and ITIM domain (TIGIT) as well as lymphocyte activation gene 3 (LAG-3, CD223)[12−14]. Blockade of these individual checkpoints may be insufficient to elicit a potent immune response[15,16]. Thus, combinational blockade of multiple immune checkpoints can be one way to increase the patient's response rates[17,18].

LAG-3 is a type I transmembrane protein expressed mainly on activated T cells as well as natural killer cells, and consists of four extracellular immunoglobulin (Ig)-like domains (D1−D4) that are highly homologous to CD4[19,20]. Studies on LAG-3 knockout mice and LAG-3 antibodies revealed that LAG-3 primarily negatively regulates the proliferation, activation, effector function and homeostasis of T cells[21−24]. It was also found that LAG-3 was constitutively expressed on regulatory T cells (Tregs) and contributed to their suppressive function[25,26]. It was reported that LAG-3 bound to major histocompatibility complex class II (MHC-II) with high affinity[27]. Currently, monoclonal antibodies that block the interaction of LAG-3 with MHC-II are undergoing clinical trials for antitumor activity[14,28]. Among them, BMS-986016 initiated Phase I clinical trials in 2013, and LAG-3 was identified as the third clinically targeted immune checkpoint with antagonistic mAb after CTLA-4 and PD-1[29]. LAG-3 and PD-1 are shown to be co-expressed on tumor-infiltrating lymphocytes of transplantable tumor models[30], and LAG-3 antibodies alone or in combination with PD-1 blockers can reduce malignant cancer cell growth and promote tumor clearance in mice tumor models[17,30,31]. In ovarian cancer patients, co-expression of LAG-3 and PD-1 was also found on antigen-specific $CD8^+$ T cells, and the co-blockade behavior promoted the T cell proliferation and facilitated cytokine release[32]. Accordingly, the combination of LAG-3 and PD-1 antibodies has entered clinical trials for various cancer entities against solid tumors. It has been reported that the combination treatment using BMS-986016 (relatlimab) and anti-PD-1 (nivolumab) has shown more promising anticancer effects in melanoma patients compared with using only anti-PD-1 therapy[29].

Currently, the mainly blocking agents of immune checkpoints are therapeutic antibodies. Antibodies have the characteristics of high specificity and significant therapeutic effects[33]. However, there are drawbacks involved, such as high immunogenicity which may cause side effects, low tumor penetration, and high treatment costs[34]. In contrast to therapeutic antibodies, peptides and small chemical compounds have smaller molecular weights, lower immunogenicity, better tissue and tumor penetration, as well as lower manufacturing costs[35−37]. Therefore, this can be a promising complement to antibody therapy, in order to achieve greater synergistic effects[38].

Compared with linear peptides, cyclic peptides have a more stable spatial structure and a longer *in vitro* half-life[39], and studies have shown that macrocyclic peptides were capable to block the PD-1/PD-L1 pathway[40]. Therefore, it demonstrates that cyclic peptides are one of the effective blockers of immune checkpoints.

In this study, by using phage display technology[41], a high-affinity cyclic peptide C25 that specifically binds to LAG-3 was firstly developed. Further, the *in vitro* and *in vivo* experiments showed that C25 could effectively block the LAG-3 signaling pathway and achieve great antitumor effects.

2. Methods and materials

2.1. Subtractive phage bio-panning

The bio-panning was performed by using a commercially available Ph.D.-C7C library (New England Biolabs, Beijing, China). The first round of bio-panning was conducted on rhLAG-3-Fc protein (Sino Biological, Beijing, China) to select all binders. Briefly, mixed 2×10^{11} pfu phages and rhLAG-3-Fc protein (2.5 μg) for 20 min at room temperature, the mixture was then added into 5 μL Protein A/G Mix Magnetic Beads (Thermo Fisher Scientific, Waltham, MA, USA) for 20 min at room temperature, the beads were blocked by 1% bovine serum albumin (BSA, Sigma−Aldrich, Shanghai, China) at 4 °C for 1 h before used. Beads were washed five times using TBST (TBS with 0.1% tween-20) and then eluted in 0.2 mol/L glycine-HCl (pH 2.2) for 20 min at room temperature. The solution was neutralized with 1 mol/L Tris−HCl (pH 9.1), then tittered and amplified according to New England Biolabs protocol. For subtractive bio-panning, 2×10^{11} pfu of the amplified eluate was first applied to 2.5 μg hIgG1-Fc protein (Sino Biological) for 20 min at room temperature,

and then added the mixture into 5 μL Protein A/G Mix Magnetic Beads for 20 min at room temperature. Finally, the mixture was centrifuged, and the supernatant was applied to rhLAG-3-Fc protein (1.5 μg at second to fourth and 1.0 μg at fifth bio-panning process). Phages were eluted from rhLAG-3-Fc protein and amplified. Subtractive bio-panning was repeated four times, using the amplified eluate from the previous cycles the starting library for each round. Plaques from the fifth round of panne were selected for DNA sequencing. The nucleotide sequences encoding for peptides on the phage clones were determined by Suzhou Genewiz Biotechnology Co., Ltd. (Suzhou, China).

2.2. Cyclic peptide synthesis

The cyclic peptides with disulfide bond were chemically synthesized by Nanjing ChenPeptide Biotech Ltd. (Nanjing, China). The molecular weights and purity were confirmed by mass spectrometry and RP-HPLC, respectively.

2.3. Affinity measurements by microscale thermophoresis (MST)

MST is an effective method for the characterization of bimolecular interaction quantity depends on the thermal motion[42]. Here MST was applied to determine the binding constants for peptides−protein interactions and used the dissociation constant (K_d) as the affinity parameter for both molecules. MST measurements were performed using the Monolith NT.115 system (NanoTemper Technologies GmhH, München, Bayern, Germany) to assess the affinity of the cyclic peptide to human LAG-3 protein. Briefly, LAG-3 protein (Sino Biological) was labeled with Red-NHS647 dye (NanoTemper Technologies GmhH), the labeling efficiency was determined by MST, and the successfully labeled protein was used for subsequent experiments. First, the cyclic peptide was diluted to 200 μmol/L with MST buffer, and 2-fold serial dilutions were carried out to obtain 16 concentration gradients subsequently. Equal volume of Red-NHS647 dye-labeled protein and peptide were incubated at room temperature for 5 min, the mixture was loaded onto standard capillaries (NanoTemper Technologies GmhH) and immediately placed in an MST instrument for detection. The dissociation constant (K_d) was determined using the NanoTemper analysis software MO. Affinity Analysis v2.2.4.

2.4. Cell lines and cell culture

Murine colorectal cancer cell lines CT26 and human myeloid leukemia mononuclear cells THP-1 were cultured in DMEM medium (GIBCO, Grand Island, NY, USA), murine melanoma cell lines B16 and B16-OVA were cultured in RPMI 1640 medium (GIBCO). DMEM and RPMI 1640 medium were supplemented with 10% FBS (Biological Industries, Kibbutz Beit HaEmek, Israel), 100 U/mL penicillin (Solarbio, Beijing, China) and 100 μg/mL streptomycin (Solarbio) at 37 °C with 5% CO_2 under fully humidified conditions.

2.5. Inducing THP-1 cell to express HLA-DR protein

THP-1 cells with a density of 4×10^5 cells/mL were cultured for 4 h in DMEM medium containing 0.3% FBS, and stimulated by 80 ng/mL of rhIFN-γ (Peprotech, Rocky hill, CT, USA) for 48 h[43]. The cells were then harvested and incubated with human HLA-DR flow antibody (eBioscience, San Diego, CA, USA) for 30 min at 4 °C and the cells were washed and analyzed by a FACS Calibur flow cytometry (BD Bioscience, San Jose, CA, USA).

2.6. Cell-based blocking assay

THP-1 cells expressing HLA-DR (represented subtype of human MHC-II) were used for cell-based blocking assay. Briefly, the assay was carried out in PBS pH 7.2, each 50 μL reaction system contained a final concentration of 0, 0.1, 1, 10 and 100 μmol/L of cyclic peptide and 400 ng of hLAG-3-Fc protein. After incubation for 30 min at 4 °C, the mixture was added to 5×10^5 THP-1 cells with further incubation at 4 °C for 30 min. Subsequently, the anti-Fc-PE antibody (eBioscience) was added and incubated at 4 °C for 30 min, and the cells were washed and analyzed by a FACS Calibur flow cytometry (BD Bioscience).

The reaction system without peptide was used as a positive control, and the system in which cells only reacted with the flow anti-Fc-PE antibody served as a negative control.

$$\text{Blocking rate}\ (\%) = \frac{\text{Positive control mean value} - \text{Experimental group mean value}}{\text{Positive control mean value}} \times 100 \quad (1)$$

2.7. PBMC function assay

Peripheral blood mononuclear cells (PBMCs) from healthy donors were separated by means of density gradient centrifugation (Tianjin Hao Yang Biological Manufacture Co., Ltd., Tianjin, China). PBMCs (2×10^5 cells/well) were cultured in 48-well flat-bottomed plates with 500 μL IMDM containing 10% FBS. The PBMCs were stimulated by 1 μg/mL anti-CD3 (eBioscience) and 0.5 μg/mL anti-CD28 antibodies (eBioscience), the activated PBMCs were incubated with 100 μmol/L peptide or 5 μg/mL anti-LAG-3 blocking antibody (Abcam, Cambridge, England) or 10 μg/mL anti-PD-1 antibody (Nivolumab, Bristol-Myers Squibb, New York, NY, USA). Protein transport inhibitor cocktail (0.5 μL, BD Bioscience) was added to each well and incubated over 4 h. Cells were collected and stained with surface markers antibodies anti-human CD4-PerCP-Cy5.5 (OKT4, eBioscience), anti-human CD8-APC (SK1, eBioscience) prior to fixation and permeabilization. Permeabilized cells were then stained with anti-human IFN-γ PE (4S.B3, eBioscience) and analyzed by FACS Calibur flow cytometry (BD Bioscience).

For cytokine detection assay, cells were incubated for 5 days, the levels of IFN-γ were evaluated by ELISA kit (eBioscience). Briefly, ELISA plate was coated with 100 μL/well of IFN-γ capture antibody overnight at 4 °C, aspirated and washed 3 times with washing buffer (PBS pH 7.2 with 0.05% Tween-20), and then blocked with ELISA/ELISPOT buffer for 1 h at room temperature. The diluted supernatant samples or IFN-γ standard were added into wells and incubated for 2 h at room temperature. Bound biotinylated IFN-γ were detected using avidin-HRP and 1 × TMB solution. Finally, stop solution of 50 μL/well was added and the

plate optical density was measured at 450 nm using an EMax Plus Microplate Reader (Molecular Devices, San Jose, CA, USA).

2.8. Mice

Six-week-old female BALB/c and C57BL/6 mice were purchased from Beijing Vital River Laboratory Animal Technology Co., Ltd. (Beijing, China). The animals had free access to food and water and were maintained in a specific pathogen free facility (24 ± 1 °C). Animal welfare and experimental procedures were carried out and approved in accordance with the Ethical Regulations on the Care and Use of Laboratory Animals of Zhengzhou University (Zhengzhou, China).

2.9. Tumor model and treatments

Female BALB/c mice were subcutaneously injected with 1×10^5 syngeneic CT26 cells to establish colorectal cancer xenograft model. Female C57BL/6 mice were subcutaneously injected with 1×10^5 syngeneic B16 or 2×10^5 syngeneic B16-OVA cells to establish melanoma xenograft model.

For depletion of indicated T cells, BALB/c mice were intraperitoneal injected with 250 μg of CD8-depleting antibody (clone: YTS.192.4) the day before CT26 tumor inoculation and every 4 days thereafter, 200 μg Rat Ig (Sigma−Aldrich) injected as control. The depletion efficacy was confirmed by the flow cytometry.

Tumor sizes were measured using a digital caliper, and tumor volumes were calculated as Eq. (2):

$$V = 1/2 \times a\ (\text{length}) \times b\ (\text{width}) \times c\ (\text{height}) \quad (2)$$

Treatment of mice was initiated after the tumors had been grown for 8−10 days until reaching a palpable size of 40−80 mm^3. Tumor bearing mice were randomly grouped, C25 was paraneoplastic injection at a dose of 2 mg/kg/day over 14 days, and normal saline (NS) was used as a negative control. The tumor volume was measured every 2 days and the body mass was weighed.

2.10. MTT assay

CT26, B16 or B16-OVA cells were seeded at 3×10^3 cells/well in 96-well plates and allowed to grow for 24 h before treatment. Then cells were treated with PBS pH 7.2 or test peptides (at concentrations of 12.5−200 μmol/L). After 24, 48, and 72 h, the cell viability was measured using 5 mg/mL MTT reagent (Sigma−Aldrich) dissolved in PBS pH 7.2 and incubated at 37 °C for 4 h. After removing incubation medium, formazan crystals were dissolved in 150 μL DMSO. Spectroscopic readings (490 nm) were taken.

2.11. $CD4^+$ T cells, $CD8^+$ T cells and $FOXP3^+$ tregs infiltration in tumor

Tumor-bearing mice were sacrificed on the last day of treatment. Tumor tissues were minced and digested in collagenase IV (Invitrogen, Carlsbad, CA, USA) and Dnase I (Sigma−Aldrich) for 30 min at 37 °C, and passed through a 70 μm cell strainer. After centrifuging, part of the cells were collected and stained with surface markers antibodies anti-mouse CD45 FITC (30-F11, eBioscience), anti-mouse CD3 PerCP-eFluor710 (17A2, eBioscience), anti-mouse CD8α PE (53−6.7, eBioscience) for 30 min at 4 °C to detect $CD4^+$ T cells and $CD8^+$ T cells.

Another part of the cells was stained with surface markers antibodies anti-mouse CD45 FITC (30-F11, eBioscience), anti-mouse CD4 APC (GK1.5, eBioscience) and anti-mouse CD25 PE (PC61.5, eBioscience) prior to fixation and permeabilization. Permeabilized cells were then stained with anti-mouse FOXP3 PE-Cy7 (FJK-16s, eBioscience) for 30 min at 4 °C to detect $FOXP3^+$ Tregs. The cells were washed and analyzed by a FACS Calibur flow cytometry.

2.12. Intracellular cytokine staining assay

Single cell suspension of mouse spleen and draining lymph node were prepared by gentle mechanical disruption, tumor-infiltrating lymphocytes (TIL) were isolated from tumor tissues. Cells from CT26 xenograft model were stimulated with 20 ng/mL Phorbol 12-myristate 13-acetate (PMA, Sigma−Aldrich) and 1 μmol/L ionomycin (Sigma−Aldrich), and cells from B16-OVA xenograft model were stimulated with 10 μg/mL $OVA_{257-264}$ peptide in the presence of protein transport inhibitor cocktail (eBioscience) for 4 h. Cells were then stained with surface markers antibodies anti-mouse CD3 PerCP-eFluor710 (17A2, eBioscience), anti-mouse CD8α APC (53−6.7, eBioscience) or anti-mouse CD4 APC (GK 1.5, eBioscience) prior to fixation and permeabilization. Permeabilized cells were then stained with anti-mouse IFN-γ PE (XMG1.2, eBioscience), analyzed by a FACS Calibur flow cytometry.

2.13. The immunogenicity and distribution of C25 in mice

To determine whether the cyclic peptide C25 has immunogenicity during the treatment, CT26 tumor bearing mice were treated with C25 or normal saline for 14 or 21 days. Naïve mice were injected as the same for 14 days.

To further determine whether the *in vivo* quantity of the peptides was affected during the treatment, after the last treatment, each mouse was injected subcutaneously around the tumor (naïve mice were injected at the same site) with 800 μg of cyclic peptide C25. The serum of each group of mice was taken at 0, 15, 30, 60, 120, 240 min. A part of the serum was mixed with a half volume of 10% $HClO_4$, and the supernatant was taken after high-speed centrifugation at 4 °C, the content of the cyclic peptide C25 was analyzed by HPLC.

The levels of mouse IgG in serum at the indicated time points were evaluated by ELISA kit (eBioscience). Briefly, ELISA plate was coated with 100 μL/well of IgG capture antibody overnight at 4 °C, aspirated and washed twice with washing buffer (PBS pH 7.2 with 0.05% Tween-20), then blocked with ELISA/ELISPOT buffer 1 h at room temperature. Serially diluted supernatant samples or IgG standard and 50 μL detection antibody were added into wells and incubated for 2 h at room temperature. Bound

Table 1 The frequency was indicated and the affinity of cyclic peptides to hLAG-3 was measured by MST.

Peptide No.	Sequence	Frequency	MST K_d (μmol/L)
C17	CNMHTPMVC	5/75	1.83 ± 1.29
C19	CNWMINKEC	4/75	5.05 ± 2.96
C25	CVPMTYRAC	2/75	0.66 ± 0.35

Data are mean ± SD, $n = 3$.

biotinylated IgG was detected using 100 μL 1 × TMB solution for 15 min at room temperature. Finally, 50 μL/well stop solution was added and the plate optical density was measured at 450 nm using an EMax Plus Microplate Reader (Molecular Devices).

To determine the tissue specificity of cyclic peptide C25, CT26 tumor bearing mice were treated with C25 or normal saline for 14 days. The day after the last treatment, each mouse was injected subcutaneously around the tumor with 800 μg of cyclic peptide C25. After 120 min of peptide injection, the heart, liver, spleen, lung, kidney and tumor of mice were separated. Tissue lysate containing protease inhibitor was added at a concentration of 1 mL/g tissue, and the tissue was ground sufficiently on ice. The tissue slurry was collected, centrifuged at high speed, and the supernatant was mixed with a half volume of 10% $HClO_4$. After precipitation, the supernatant was harvested after high-speed centrifugation at 4 °C, and the content of the cyclic peptide C25 was analyzed by HPLC.

2.14. *Statistical analysis*

The data was shown as means ± standard deviation (SD) and statistical significance between groups was determined by Student's t test. P values < 0.05 were considered statistically significant. $^{*}P < 0.05$, $^{**}P < 0.01$, and $^{***}P < 0.001$.

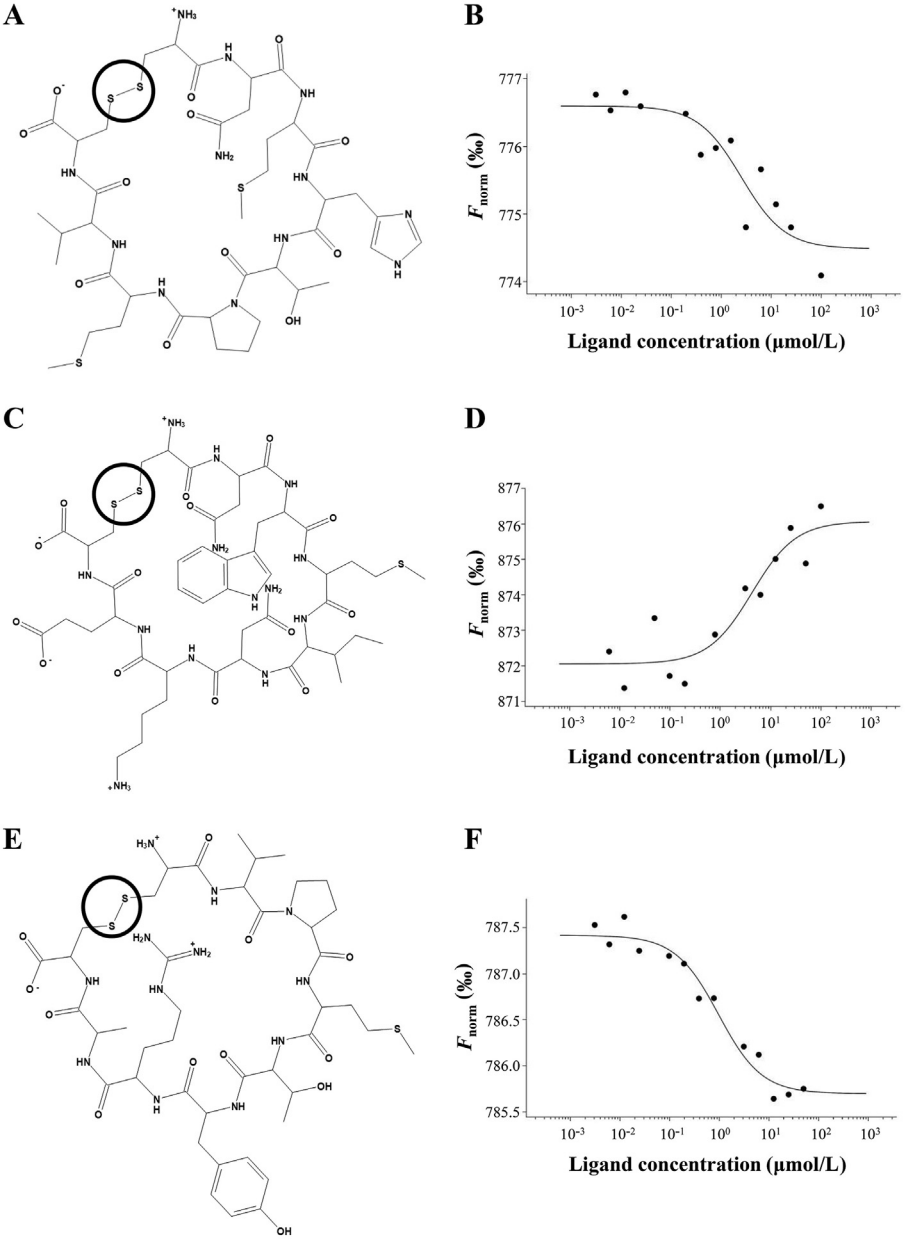

Figure 1 Binding detection of cyclic peptides to hLAG-3 by MST. Chemical structures of cyclic peptide (A) C17, (C) C19 and (E) C25, the disulfide bond that forms the peptide into cyclic was identified within the circle. The MST binding curves of cyclic peptide (B) C17, (D) C19 and (F) C25 to hLAG-3.

3. Results

3.1. Phage display screening

To obtain the LAG-3 binding peptides, 5 rounds of bio-panning on the rhLAG-3-Fc protein were performed, and the phage clones were randomly selected. A total of 75 efficient nucleotide sequences were obtained, and the amino acid sequences with the enriched phage clones were shown in Table 1. The three peptides (C17, C19 and C25) were synthesized.

3.2. Affinity measurement between cyclic peptides and LAG-3 protein

The MST binding curves of cyclic peptide C17, C19 and C25 to hLAG-3 were shown in Fig. 1B, D and F. The K_d values for the binding of C17, C19 and C25 to hLAG-3 were shown in Table 1. The results showed that C25 had the highest affinity among these three peptides with the K_d value of 0.66 μmol/L.

The SPR binding curves and K_d values of cyclic peptide C17, C19 and C25 to hLAG-3 were shown in Supporting Information Figs. S1A–C. Consistent with the results of MST, C25 showed the highest affinity with the K_d value of 0.215 μmol/L.

3.3. C25 impaired the interaction of LAG-3 and HLA-DR

To further identify whether C25 could block the interaction of LAG-3 and HLA-DR, a ligand inhibition assay and a cell-based analysis were performed to investigate the interference of C25 on LAG-3 binding to HLA-DR (Fig. 2A). First, the expression of HLA-DR on THP-1 cells were induced with different concentrations (0–100 ng/mL) of rhIFN-γ for 48 h, and HLA-DR expression was monitored by a flow cytometry. As shown in Fig. 2B, the concentration of rhIFN-γ was determined to be 80 ng/mL. Cell-based blocking assays showed that cyclic peptide C25 had the highest efficacy to block HLA-DR/LAG-3 among these three peptides. As shown in Fig. 2C, C25 effectively blocked the binding of LAG-3 to HLA-DR in a dose-dependent manner. With the increased concentration of C25, the fluorescence signals decreased. At 10 μmol/L, the blocking rate of C25 exceeded 40%, when the concentration reached 100 μmol/L, the blocking rate could reach 60% (Fig. 2C and D).

3.4. C25 activated CD8$^+$ T cells in vitro depends on LAG-3

LAG-3 could be inducible expressed on peripheral CD4$^+$ and CD8$^+$ T cells upon activation. To verify whether C25 can activate T cells *in vitro*, PBMCs from the blood of healthy donor were isolated, CD3 and CD28 antibody were added to stimulate T cells and incubated with PBS or C25. The IFN-γ secretion by the cells was measured using ELISA. The IFN-γ production in PBMC cells was significantly enhanced when treated with C25 (100 μmol/L, Fig. 3A). At the same time, we detected the percentage of CD8$^+$ and CD4$^+$ T cells producing IFN-γ in each T-cell subset by a flow cytometry. As shown in Fig. 3B–E, C25 increased the percentage of CD8$^+$ IFN-γ$^+$ (Fig. 3B and C) but not that of CD4$^+$ IFN-γ$^+$ (Fig. 3D and E) compared with the control. After blocking the LAG-3 protein with the anti-LAG-3 antibody, C25 could no longer enhance IFN-γ release and CD8$^+$ T cells activation (Fig. 3A and

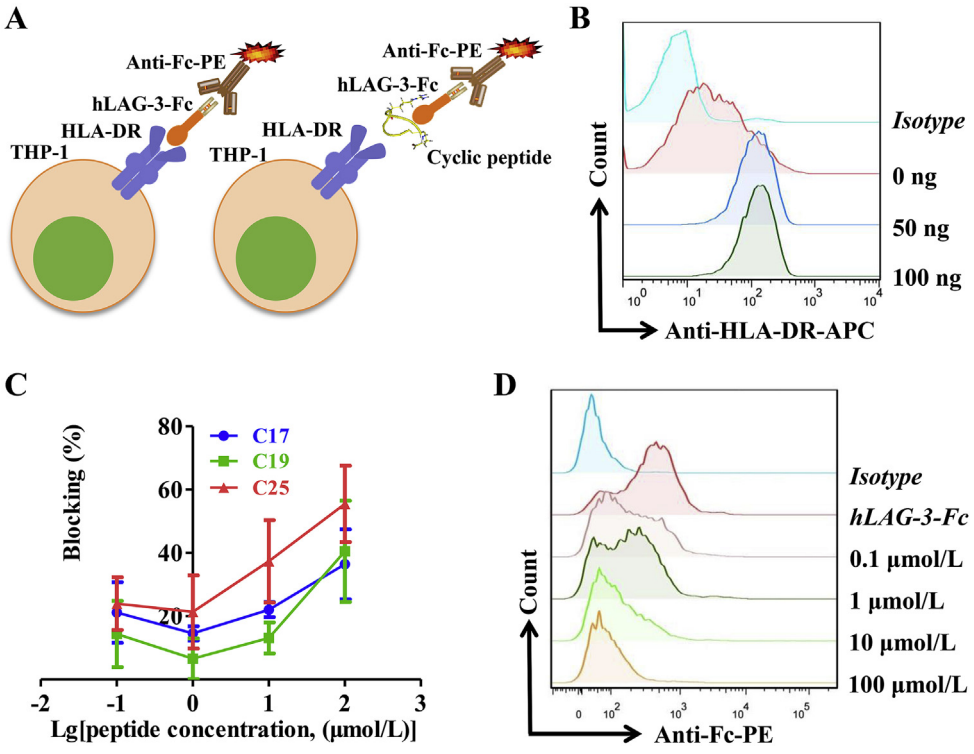

Figure 2 The effect of cyclic peptides on LAG-3/HLA-DR interaction was determined *via* cell-based blocking assay. (A) Schematic diagram of cell-based blocking assay. (B) Flow cytometry analysis of HLA-DR on THP-1 cells induced by different concentrations (0–100 ng/mL) of rhIFN-γ for 48 h. (C) Cell-based blocking assay of different concentrations of cyclic peptides C17, C19 and C25. (D) A representative flow diagram of LAG-3/HLA-DR blocking by different concentrations of cyclic peptide C25. Data are expressed as the mean ± SD (n = 3).

C). Overall, these results indicated that C25 could recover the function of $CD8^+$ T cells *in vitro* by acting on LAG-3.

3.5. C25 did not impact tumor cells proliferation

To evaluate the direct killing effects of C25 on CT26, B16 and B16-OVA tumor cells, MTT assays were conducted. C25 showed no significant effects on proliferation (Figs. 4A, 7A and 8A) when compared with the control (PBS, pH 7.2).

3.6. C25 could inhibit CT26 tumor growth via a T-cell dependent manner

To identify the *in vivo* effects of C25, CT26 tumor bearing mice were treated with C25 (2 mg/kg/day) for 14 days. The results showed that C25 could significantly inhibit the growth of the established CT26 tumors (Fig. 4B and C). However, the C25 did not show pronounced killing effects on CT26 tumor cells (Fig. 4A), therefore, this can be deduced that C25 might function by activating the body immunity. The infiltration of $CD8^+$ T cells, $CD4^+$ T cells and $FOXP3^+$ Tregs were detected in tumors. As a result, the infiltration of $CD8^+$ and $CD4^+$ T cells in the C25 group significantly increased compared with the control group (Fig. 5A–C), and the infiltration of $FOXP3^+$ Tregs in the C25 group significantly decreased (Fig. 5D and E). The percentages of IFN-γ producing $CD8^+$ and $CD4^+$ T cells in the spleen, draining lymph node and TIL were determined. The results showed that the ratio of $CD8^+$ IFN-γ^+ T cells in the C25 group increased compared with the control group (Fig. 5F, G, J and K), while the ratio of $CD4^+$ IFN-γ^+ T cells had no significant differences (Fig. 5H, I, L and M). All these results indicated that C25 was capable to inhibit CT26 tumor growth *via* a $CD8^+$ T cell dependent mechanism.

3.7. Anti-tumor effect of C25 mainly depends on $CD8^+$ T cells

Further, $CD8^+$ T cells depleting model was established to verify the role of $CD8^+$ T cells in the process of tumor inhibition by C25. In the $CD8^+$ T cells depletion mouse model, the tumor grew rapidly and C25 treatment showed no obvious effects on the tumor growth compared with the control group (Fig. 6A and B), indicating that the C25 functioned to inhibit tumor growth dependent on the activation of $CD8^+$ T cells.

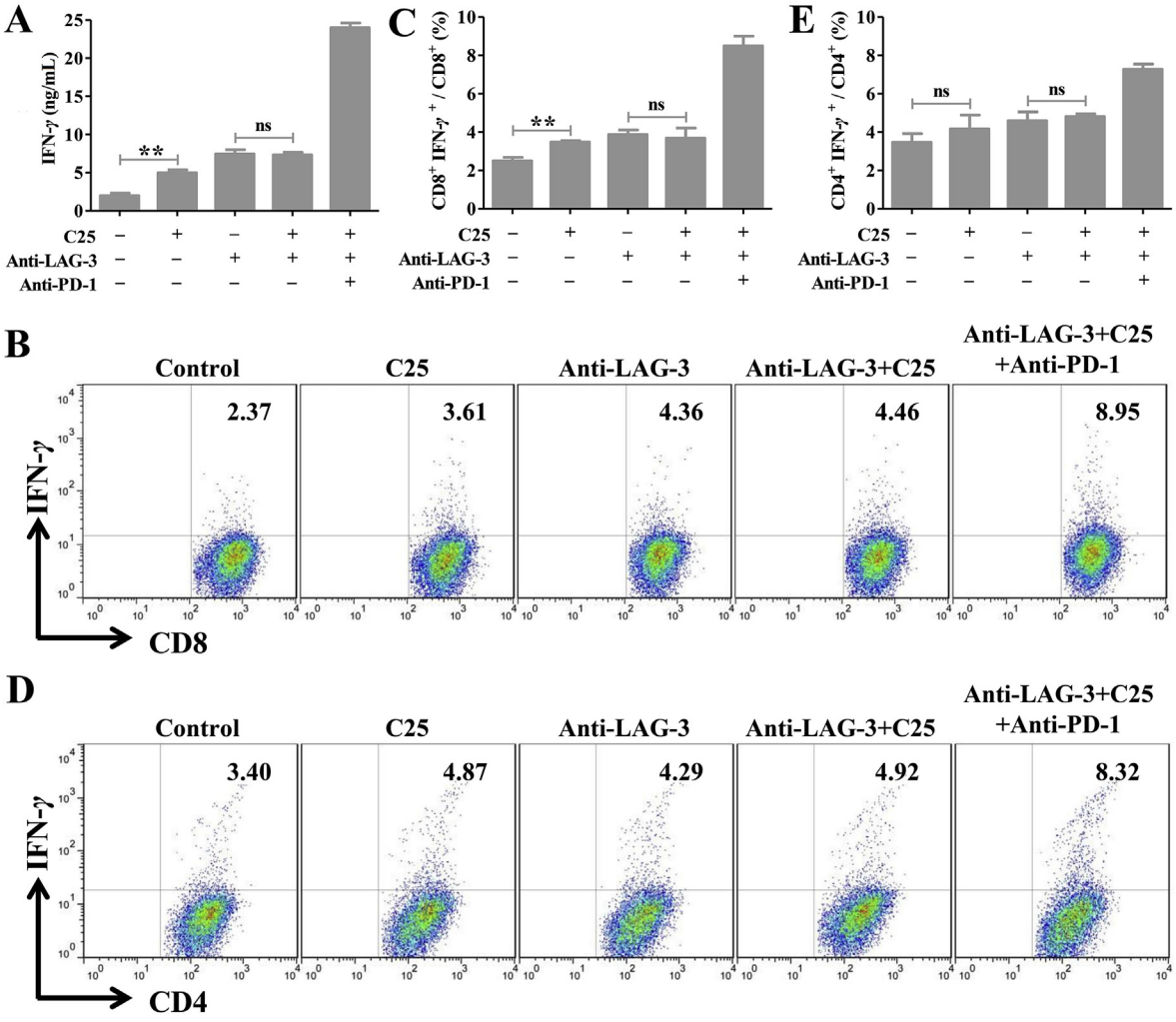

Figure 3 The activation of cyclic peptide C25 on $CD8^+$ T cells was determined *in vitro*. (A) Cyclic peptide C25 has the function of stimulating secretion of IFN-γ by human PBMCs. Effects of cyclic peptide C25 on the percentage of (B and C) $CD8^+$ IFN-γ^+ T cells and (D and E) $CD4^+$ IFN-γ^+ T cells. Data are expressed as the mean ± SD ($n = 3$) and statistical significance between groups was determined by Student's *t* test: $^{**}P < 0.01$; ns, not significant.

3.8. C25 could inhibit B16 tumor growth

To further evaluate the anti-tumor effect of C25, B16 xenograft mouse model with a more malignant phenotype was used. The results showed that C25 could significantly inhibit the growth of B16 tumors (Fig. 7B and C). However, at the later stage, the growth of the tumor gradually deviated from the inhibition of the C25 and the tumor started to grow rapidly. In this model, it demonstrated C25 might only play a role in delaying tumor development. We speculated that B16 cells could be stimulated by inflammatory factors such as IFN-γ in tumor microenvironment to express PD-L1 which thus mediate immune escape through the PD-1/PD-L1 pathway.

3.9. C25 killed B16-OVA tumor cells by antigen-specific $CD8^+$ T cells reaction

To verify whether C25 was capable of eliciting antigen-specific $CD8^+$ T cell responses, a B16-OVA xenograft mouse model was established. The results showed that the C25 treatment significantly reduced the tumor size (Fig. 8B). The results of infiltration of $CD8^+$ T cells and $Foxp3^+$ Tregs in tumors showed that the $CD8^+$ T cell infiltration in the C25 group significantly increased (Fig. 8C and D), while the infiltration of $FOXP3^+$ Tregs significantly reduced (Fig. 8E and F). In the isolated spleen, draining lymph nodes cells and TIL, the proportion of antigen-specific $CD8^+$ IFN-γ^+ T cells stimulated by $OVA_{257-264}$ peptide significantly increased with the treatment of C25 (Fig. 8G, H, I and J). These results indicated that the promising tumor inhibition effect of C25 may result from the increasing of $CD8^+$ T cells infiltration and decreasing of $FOXP3^+$ Tregs infiltration in tumors, and effectively triggering antigen-specific $CD8^+$ T cell responses to kill tumor cells.

3.10. The immunogenicity and distribution of C25 in mice

The immunogenicity of C25 was assessed in mice with or without CT26 xenograft. The results showed that the IgG levels in the blood of naïve mice, tumor bearing mice after 14 days of C25 treatment were not significantly different from those in the control group, indicating that C25 did not cause significant immune response in mice, as shown in Supporting Information Fig. S2A. At the same time, we examined the elimination of peptide C25 in mice, and found that the elimination of C25 between naïve mice and tumor bearing mice showed no significant difference, regardless of the C25 treatment for 14 days, as shown in Fig. S2B.

The distribution of peptide in normal tissues and tumors in mice after 120 min treatment with peptide C25 was analyzed by HPLC. It was found that peptide mainly distributed in tumors and livers, as shown in Fig. S2C, indicating that peptide C25 had good tumor penetration.

4. Discussion

With the gradual deepening of the immune checkpoints of CTLA-4 and PD-1/PD-L1 and the approval of their blocking antibodies for the treatment of various tumors, other immune checkpoints as TIM3, TIGIT and LAG-3 also attract great attention[12–14]. Ongoing clinical trials are not only combined different immune checkpoints, but also combined with radiation therapy, chemotherapy, or cancer vaccines, in order to achieve synergistic therapeutic effects. LAG-3 is considered as a promising immune checkpoint[44], the combination of anti-LAG-3 (relatlimab) and anti-PD-1 (nivolumab) exhibited exciting efficacy in melanoma patients with resistance to the previous anti-PD-1/PD-L1 therapy (NCT01968109). Most importantly, the combination therapy

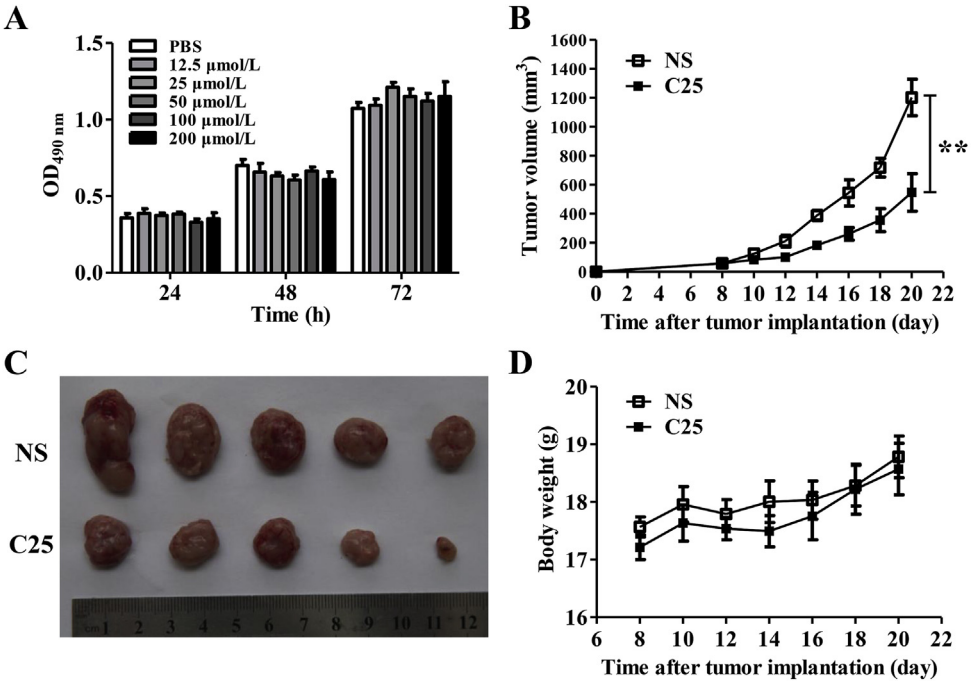

Figure 4 Cyclic peptide C25 could inhibit CT26 tumor growth not directly killing tumor cells. (A) MTT analysis of the effect of cyclic peptide C25 on the proliferation of CT26 tumor cells *in vitro*. CT26 xenograft mice model was established, cyclic peptide C25 (2 mg/kg/day) was treated for 14 days when the tumor grew to 40–80 mm^3. The (B) tumor volumes, (C) tumor sizes and (D) body weight of cyclic peptide C25 and control group. Data are expressed as the mean ± SD ($n = 5$) and statistical significance between groups was determined by Student's *t* test: $^{**}P < 0.01$.

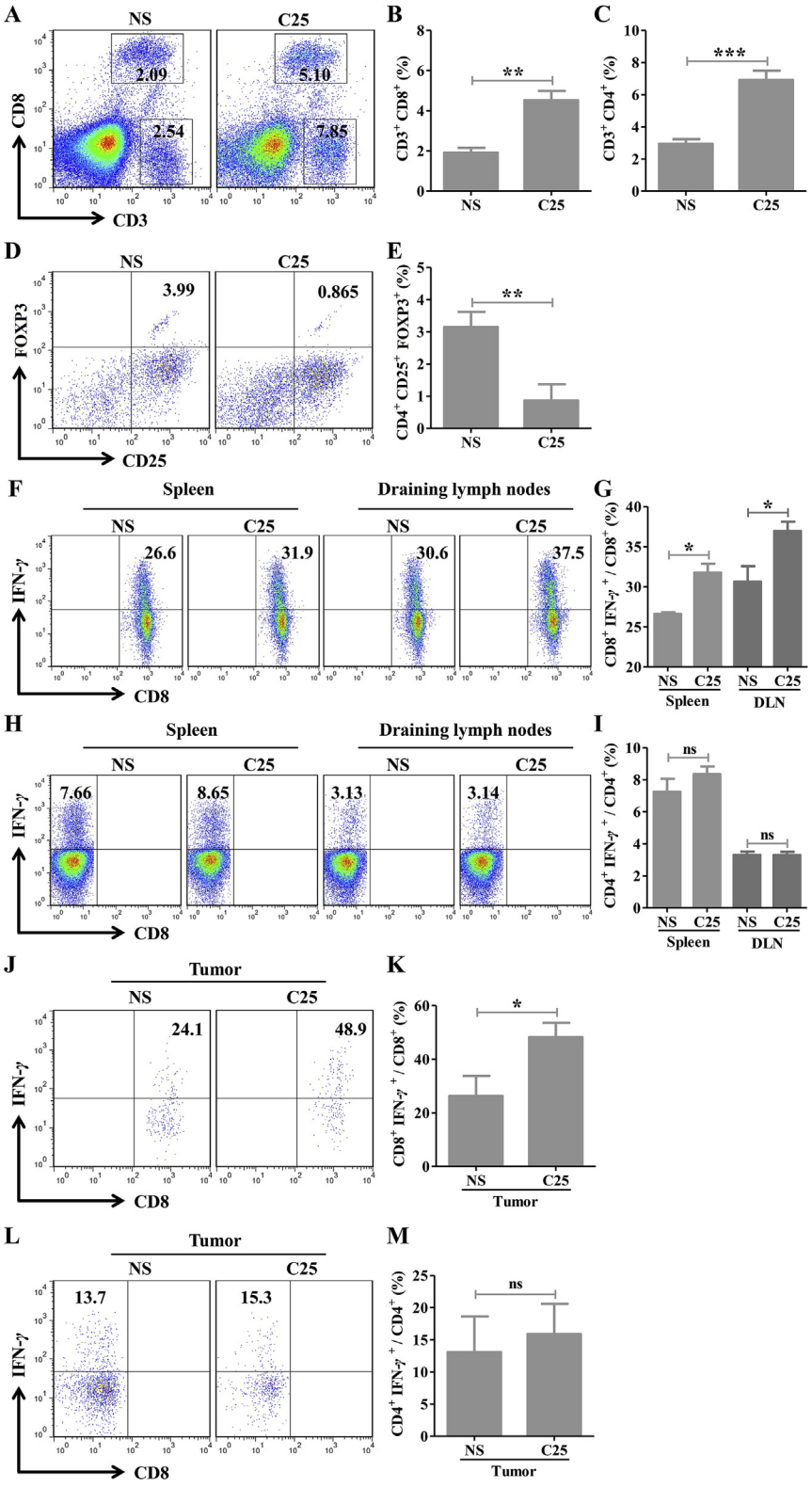

Figure 5 Cyclic peptide C25 inhibits CT26 tumor growth by activating $CD8^+$ T cells and reducing $FOXP3^+$ Tregs. Tumor, spleen and draining lymph nodes were isolated from tumor bearing mice. (A and B) $CD8^+$ T cells infiltration, (A and C) $CD4^+$ T cells infiltration and (D and E) $Foxp3^+$ Tregs infiltration in cyclic peptide C25 and control group ($n = 4$). The ratio of (F and G) $CD8^+$ IFN-γ^+ T cells and (H and I) $CD4^+$ IFN-γ^+ T cells in the spleen and draining lymph nodes ($n = 5$). The ratio of (J and K) $CD8^+$ IFN-γ^+ T cells and (L and M) $CD4^+$ IFN-γ^+ T cells in the tumors ($n = 4$). Data are expressed as the mean ± SD and statistical significance between groups was determined by Student's t test: $^*P < 0.05$, $^{**}P < 0.01$, $^{***}P < 0.001$; ns, not significant.

showed a safety profile similar to that of nivolumab monotherapy with rare grade of 3/4 adverse events[45].

In this study, a cyclic peptide C25 with high affinity to the human LAG-3 protein by phage display was identified. The results showed that the affinity K_d values of C25 and human LAG-3 protein was 0.66 μmol/L by MST and 0.215 μmol/L by SPR, indicating that C25 could effectively bind with LAG-3. In addition to the effective interaction with LAG-3, it is essential to identify the blocking efficiency of the molecule in the binding of LAG-3 with the ligands. Thus, we measured the blocking ability of the C25 by cell-based blocking assay and found that C25 could block the HLA-DR from binding to LAG-3 in a dose-dependent manner. In addition, when the concentration of C25 was at 100 μmol/L, the blocking rate achieved up to 60%, indicating that the C25 could effectively block the LAG-3/HLA-DR protein interactions. The LAG-3 protein consists of four Ig-like extracellular domains, D1−D4[19,20]. MHC-II interacts with LAG-3 *via* the D1 domain of the LAG-3 protein[19]. Our study found that C25 could block the binding of LAG-3 to MHC-II, therefore, we hypothesized that C25 might bind to the D1 region of LAG-3, occupying the key site of MHC-II and preventing the binding of LAG-3 to MHC- II.

The clinical efficacy of tumor immunotherapy by using immune checkpoint blockers depends on the activation and expansion of tumor-infiltrating $CD8^+$ T cells[46,47]. LAG-3 acts as a negative regulator of T cells and has a direct inhibitory effect on $CD8^+$ T cells[22,24,48]. LAG-3 is expressed at a lower level on unactivated $CD8^+$ T cells[49] but overexpressed in tumor-infiltrating $CD8^+$ T cells, such as in hepatocellular carcinoma, renal cell

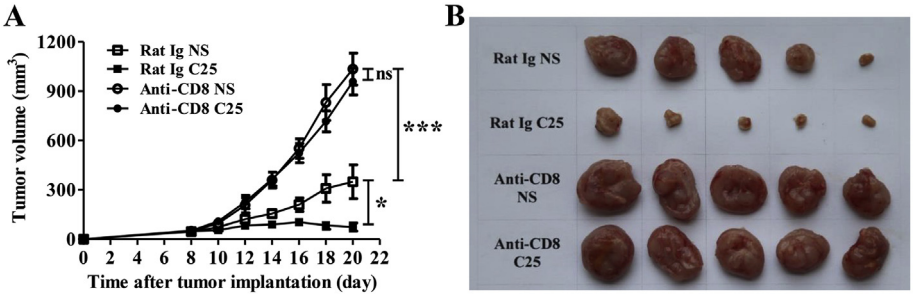

Figure 6 Effect of cyclic peptide C25 on CT26 tumor cells after depletion $CD8^+$ T cells in mice. BALB/c mice were intraperitoneal injected with 250 μg of CD8-depleting antibody the day before CT26 tumor inoculation and every four days thereafter, 200 μg Rat Ig as control. Cyclic peptide C25 (2 mg/kg/day) was treated for 14 days when the tumor grew to 40−80 mm^3. The (A) tumor volumes and (B) tumor sizes after $CD8^+$ T cell deletion. Data are expressed as the mean ± SD ($n = 5$) and statistical significance between groups was determined by Student's t test: $^*P < 0.05$, $^{***}P < 0.001$; ns, not significant.

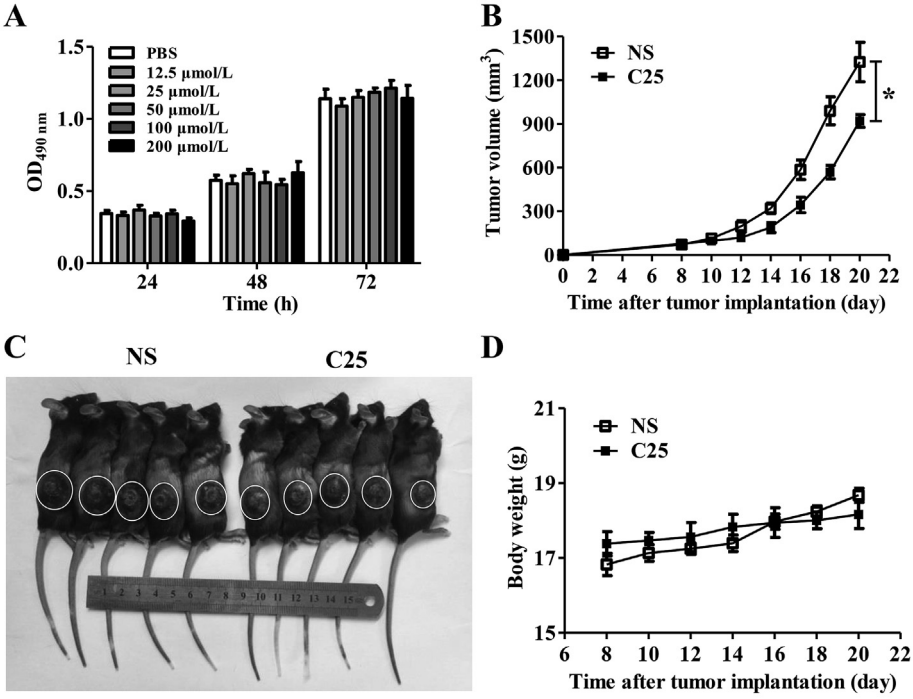

Figure 7 Cyclic peptide C25 could inhibit B16 tumor growth by not directly killing tumor cells. (A) MTT analysis of the effect of cyclic peptide C25 on the proliferation of B16 tumor cells *in vitro*. B16 xenograft mice model was established, cyclic peptide C25 (2 mg/kg/day) was treated for 14 days when the tumor grew to 40−80 mm^3. (B) Tumor volumes, (C) Tumor sizes, and (D) Body weight of cyclic peptide C25 group and the control group. Data are expressed as the mean ± SD ($n = 5$) and statistical significance between groups was determined by Student's t test: $^*P < 0.05$.

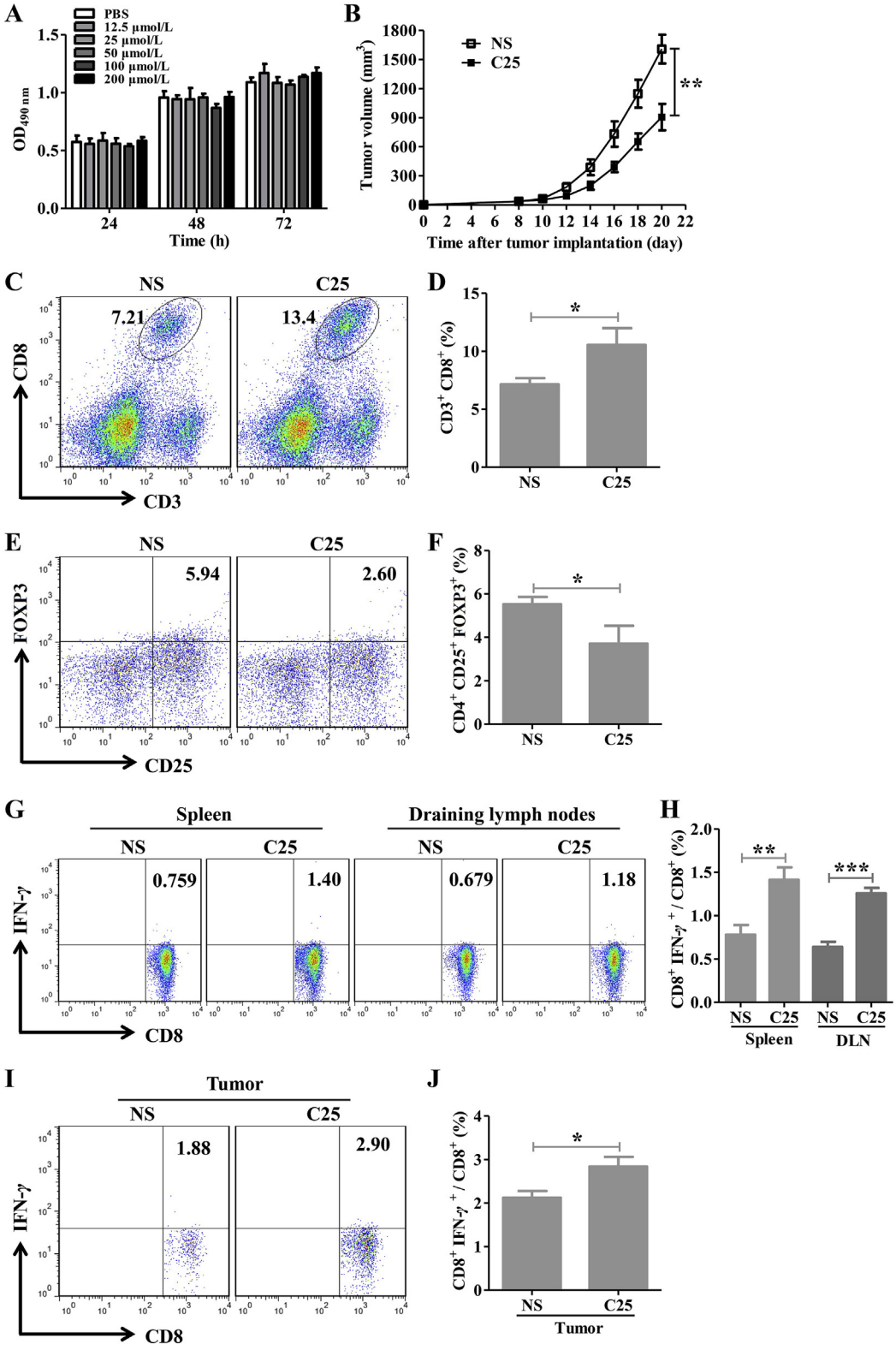

Figure 8 Cyclic peptide C25 kills B16-OVA tumor cells by antigen-specific $CD8^+$ T cell reaction and $FOXP3^+$ Tregs decreased. B16-OVA xenograft mice model was established, cyclic peptide C25 (2 mg/kg/day) was treated for 14 days when the tumor grew to 40−80 mm^3. (A) MTT analysis of the effect of cyclic peptide C25 on the proliferation of B16-OVA tumor cells *in vitro* ($n = 5$). (B) The tumor volumes of mice ($n = 5$). The (C and D) $CD8^+$ T cells ($n = 5$) and (E and F) $FOXP3^+$ Tregs infiltration ($n = 4$) in cyclic peptide C25 and control group. (G and H) The ratio of $CD8^+$ IFN-γ^+ T cells in the spleen and draining lymph nodes ($n = 4$). (I and J) The ratio of $CD8^+$ IFN-γ^+ T cells in the tumors ($n = 4$). Data are expressed as the mean ± SD and statistical significance between groups was determined by Student's *t* test: $^*P < 0.05$, $^{**}P < 0.01$, $^{***}P < 0.001$.

carcinoma and other solid tumors[50]. In self-tolerance models, LAG-3 blockade enhances the effector function of $CD8^+$ T cells and release more IFN-γ[24]. Treatment of melanoma tumor model with LAG-3 antibody can result in an increase of $CD8^+$ IFN-γ producing cells and a reduction in tumor growth[30]. In our study, the ratio of tumor-infiltrating $CD8^+$ T cells in CT26 xenograft mouse models increased after treatment with C25 peptide, and the proportion of $CD8^+$ IFN-γ^+ T cells in the spleen and draining lymph nodes also significantly increased. In B16-OVA xenograft mouse models, the ratio of tumor-infiltrating $CD8^+$ T cells increased after treatment with C25 peptide. We stimulated T cells *in vitro* using $OVA_{257\text{-}264}$ peptide which capable of causing peptide-specific antigen T cells response, and found that the proportion of IFN-γ^+ $CD8^+$ T cells in the spleen, draining lymph nodes and tumors also significantly increased. Based on the above results, C25 treatment could reactivate $CD8^+$ T cells.

MHC-II, is a shared ligand for CD4 and LAG-3, and the LAG-3/MHC−II interaction can negatively regulate the expansion of $CD4^+$ T cells and inhibit the cytokine response[21,31]. Tumor-infiltrating $CD4^+$ T cells showed up-regulation of LAG-3 expression during tumor progression, with a gradual depletion feature[38]. LAG-3 blockade may potentially affect the $CD4^+$ T cell population, resulting in a relative skew of the Treg phenotype[51]. In the mice tumors treated with cyclic peptide C25, the number of tumor-infiltrating $CD4^+$ T cells was significantly increased, which should attenuate the inhibitory effect of LAG-3 on CD4 T amplification with LAG-3 blockade. However, in the isolated spleen and draining lymph node cells, there was no significant change in the proportion of activated $CD4^+$ T cells ($CD4^+$ IFN-γ^+ T cells), which was consistent with the previous *in vitro* experiment that C25 could not activate $CD4^+$ T cells in PBMCs. The results demonstrated that the blockade of LAG-3 signaling may not be the main influencing factor for activation of $CD4^+$ T cells.

In tumor microenvironment, Tregs belong to a subset of CD4 T cells that worsen the anti-tumor immune responses and Tregs can damage the production of tumor killing cytokines and inhibit the activity of the immune system[52]. The accumulation of Tregs in tumors is associated with poor prognosis in many malignancies[53]. LAG-3 is highly expressed in regulatory Tregs and is critical for Tregs to trigger maximum inhibition[25]. Recent studies have found that LAG-3 could promote Treg differentiation, LAG-3 blockade could reduce the inhibitory function of Tregs as well as promote the activity of effector T cells[51,54]. In addition, the expression of FOXP3 is considered as the most reliable marker of Tregs[26]. Therefore, in our study, we examined the change in the proportion of tumor-infiltrating $CD4^+$ $CD25^+$ $FOXP3^+$ Tregs after treatment with cyclic peptide C25. The results showed that post 14 days of C25 treatment, the tumor size of the mice significantly reduced, and the proportion of tumor-infiltrating Tregs significantly decreased. We conclude that LAG-3 blockade by the cyclic peptide C25, Tregs mediated immunosuppression can be attenuated by reducing the proportion. The decreased proportion of Tregs may be due to the LAG-3 inhibition skews CD4 cells away from Treg phenotype[51].

The above results showed that the cyclic peptide C25 had promising antitumor effect. However, peptides have inherent disadvantages relative to blocking antibodies, they are easily degraded by enzymes in plasma or cleared by glomeruli in the body, resulting in short half-lives[35]. In our study, the first and last amino acids of a peptide are both cysteine, which allows the peptide to form a ring by generating a disulfide bond between the amino acids. Cyclic peptides can theoretically slow down the *de novo* degradation of enzymes, suggesting that their anti-enzymatic ability is better than linear peptides[39]. Our studies demonstrated that cyclic peptides that bind PD-1 have better stability *in vitro* than linear peptides of the same sequence (data not shown). In fact, the degradation of peptides in the body is not necessarily a bad event, it avoids excessive immune response in the body to produce a "cytokine storm". Therefore, to appropriately prolong the retention time of the peptide rather than infinitely extending the retention time is crucial. Meanwhile, phage display technology is an effective means of high throughput screening for specific targets[41]. Our research demonstrates that cyclic peptides with high affinity can be screened for negative regulatory proteins such as PD-1. If the cyclic peptide is effective in blocking ligand and receptor interaction, it may become an effective molecule that blocks the negative regulatory signaling pathway and activates the immune response.

5. Conclusions

This study has developed a novel cyclic peptide C25 targeting LAG-3 by phage display bio-panning. The C25 peptide binds to the LAG-3 protein with high affinity *in vitro* and is capable of preventing the binding of LAG-3 to its ligands HLA-DR. The phenomenon of anti-tumor immune activity is expected *in vivo* by the evidence of $CD8^+$ T cells activation and the reduction of Tregs. Therefore, our findings provide a novel candidate peptide and strategy targeting LAG-3 for cancer immunotherapy.

Acknowledgments

This work was supported by the National Natural Science Foundation of China (No. 81822043, U1604286), Key Scientific Research Projects of Henan Higher Education Institutions (No. 18A180033).

Author contributions

Yuanming Qi and Yanfeng Gao conceived and designed the experiments. Wenjie Zhai performed the experiments. Xiuman Zhou, Hongfei Wang and Wanqiong Li helped to perform the experiments. Wenjie Zhai, Yuanming Qi and Yanfeng Gao analyzed and interpreted the results. Wenjie Zhai, Xiuman Zhou, Guanyu Chen, Xinghua Sui, Guodong Li, Yuanming Qi and Yanfeng Gao wrote the manuscript with inputs from all authors. All authors discussed the results and gave final approval of the manuscript.

Conflicts of interest

The authors declare no conflicts of interest.

Appendix A. Supporting Information

Supporting data to this article can be found online at https://doi.org/10.1016/j.apsb.2020.01.005.

References

1. Gravitz L. Cancer immunotherapy. *Nature* 2013;**504**:S1.
2. Couzin-Frankel J. Breakthrough of the year 2013. Cancer immunotherapy. *Science* 2013;**342**:1432−3.

3. Hodi FS, O'Day SJ, McDermott DF, Weber RW, Sosman JA, Haanen JB, et al. Improved survival with ipilimumab in patients with metastatic melanoma. *N Engl J Med* 2010;**363**:711−23.
4. Ferris RL, Blumenschein Jr G, Fayette J, Guigay J, Colevas AD, Licitra L, et al. Nivolumab for recurrent squamous-cell carcinoma of the head and neck. *N Engl J Med* 2016;**375**:1856−67.
5. Nghiem PT, Bhatia S, Lipson EJ, Kudchadkar RR, Miller NJ, Annamalai L, et al. PD-1 blockade with pembrolizumab in advanced merkel-cell carcinoma. *N Engl J Med* 2016;**374**:2542−52.
6. Migden MR, Rischin D, Schmults CD, Guminski A, Hauschild A, Lewis KD, et al. PD-1 blockade with cemiplimab in advanced cutaneous squamous-cell carcinoma. *N Engl J Med* 2018;**379**:341−51.
7. Socinski MA, Jotte RM, Cappuzzo F, Orlandi F, Stroyakovskiy D, Nogami N, et al. Atezolizumab for first-line treatment of metastatic nonsquamous NSCLC. *N Engl J Med* 2018;**378**:2288−301.
8. D'Angelo SP, Russell J, Lebbe C, Chmielowski B, Gambichler T, Grob JJ, et al. Efficacy and safety of first-line avelumab treatment in patients with stage IV metastatic merkel cell carcinoma: a preplanned interim analysis of a clinical trial. *JAMA Oncol* 2018;**4**:e180077.
9. Massard C, Gordon MS, Sharma S, Rafii S, Wainberg ZA, Luke J, et al. Safety and efficacy of durvalumab (MEDI4736), an anti-programmed cell death ligand-1 immune checkpoint inhibitor, in patients with advanced urothelial bladder cancer. *J Clin Oncol* 2016;**34**:3119−25.
10. Zhao X, Subramanian S. Intrinsic resistance of solid tumors to immune checkpoint blockade therapy. *Cancer Res* 2017;**77**:817−22.
11. Topalian S, Hodi F, Brahmer J, Gettinger S, Smith D, McDermott D, et al. Safety, activity, and immune correlates of anti-PD-1 antibody in cancer. *N Engl J Med* 2012;**366**:2443−54.
12. Turnis ME, Andrews LP, Vignali DA. Inhibitory receptors as targets for cancer immunotherapy. *Eur J Immunol* 2015;**45**:1892−905.
13. Baumeister SH, Freeman GJ, Dranoff G, Sharpe AH. Coinhibitory pathways in immunotherapy for cancer. *Annu Rev Immunol* 2016;**34**:539−73.
14. Anderson AC, Joller N, Kuchroo VK. Lag-3, Tim-3, and TIGIT: co-inhibitory receptors with specialized functions in immune regulation. *Immunity* 2016;**44**:989−1004.
15. Thommen DS, Schreiner J, Muller P, Herzig P, Roller A, Belousov A, et al. Progression of lung cancer is associated with increased dysfunction of T cells defined by coexpression of multiple inhibitory receptors. *Cancer Immunol Res* 2015;**3**:1344−55.
16. Rotte A, Jin JY, Lemaire V. Mechanistic overview of immune checkpoints to support the rational design of their combinations in cancer immunotherapy. *Ann Oncol* 2018;**29**:71−83.
17. Wierz M, Pierson S, Guyonnet L, Viry E, Lequeux A, Oudin A, et al. Dual PD1/LAG3 immune checkpoint blockade limits tumor development in a murine model of chronic lymphocytic leukemia. *Blood* 2018;**131**:1617−21.
18. Harris-Bookman S, Mathios D, Martin AM, Xia Y, Kim E, Xu H, et al. Expression of LAG-3 and efficacy of combination treatment with anti-LAG-3 and anti-PD-1 monoclonal antibodies in glioblastoma. *Int J Cancer* 2018;**143**:3201−8.
19. Huard B, Mastrangeli R, Prigent P, Bruniquel D, Donini S, El-tayar N, et al. Characterization of the major histocompatibility complex class II binding site on LAG-3 protein. *Proc Natl Acad Sci U S A* 1997;**94**:5744−9.
20. Triebel F, Jitsukawa S, Baixeras E, Roman-Roman S, Genevee C, Viegas-Pequignot E, et al. LAG-3, a novel lymphocyte activation gene closely related to CD4. *J Exp Med* 1990;**171**:1393−405.
21. Huard B, Hercend T, Tournier M, Triebel Fr, Faure F. Lymphocyte-activation gene 3/major histocompatibility complex class II interaction modulates the antigenic response of $CD4^+$ T lymphocytes. *Eur J Immunol* 1994;**24**:3216−21.
22. Workman CJ, Cauley LS, Kim IJ, Blackman MA, Woodland DL, Vignali DAA. Lymphocyte activation gene-3 (CD223) regulates the size of the expanding T cell population following antigen activation *in vivo*. *J Immunol* 2004;**172**:5450−5.
23. Workman CJ, Vignali DAA. Negative regulation of T cell homeostasis by lymphocyte activation gene-3 (CD223). *J Immunol* 2005;**174**:688−95.
24. Grosso JF, Kelleher CC, Harris TJ, Maris CH, Hipkiss EL, Marzo AD, et al. LAG-3 regulates $CD8^+$ T cell accumulation and effector function in murine self- and tumor-tolerance systems. *J Clin Investig* 2007;**117**:3383−92.
25. Huang CT, Workman CJ, Flies D, Pan X, Marson AL, Zhou G, et al. Role of LAG-3 in regulatory T cells. *Immunity* 2004;**21**:503−13.
26. Camisaschi C, Casati C, Rini F, Perego M, De Filippo A, Triebel F, et al. LAG-3 expression defines a subset of $CD4^+$ $CD25^{high}$ $Foxp3^+$ regulatory T cells that are expanded at tumor sites. *J Immunol* 2010;**184**:6545−51.
27. Baixeras E, Huard B, Miossec C, Jitsukawa S, Martin M, Hercend T, et al. Characterization of the lymphocyte activation gene 3-encoded protein. A new ligand for human leukocyte antigen class II antigens. *J Exp Med* 1992;**176**:327−37.
28. Andrews LP, Marciscano AE, Drake CG, Vignali DA. LAG3 (CD223) as a cancer immunotherapy target. *Immunol Rev* 2017;**276**:80−96.
29. Ascierto PA, Bono P, Bhatia S, Melero I, Nyakas MS, Svane I-M, et al. Efficacy of BMS-986016, a monoclonal antibody that targets lymphocyte activation gene-3 (LAG-3), in combination with nivolumab in pts with melanoma who progressed during prior anti-PD-1/PD-L1 therapy (mel prior IO) in all-comer and biomarker-enriched populations. *Ann Oncol* 2017;**28**:611−2.
30. Woo SR, Turnis ME, Goldberg MV, Bankoti J, Selby M, Nirschl CJ, et al. Immune inhibitory molecules LAG-3 and PD-1 synergistically regulate T-cell function to promote tumoral immune escape. *Cancer Res* 2012;**72**:917−27.
31. Goding SR, Wilson KA, Xie Y, Harris KM, Baxi A, Akpinarli A, et al. Restoring immune function of tumor-specific $CD4^+$ T cells during recurrence of melanoma. *J Immunol* 2013;**190**:4899−909.
32. Matsuzaki J, Gnjatic S, Mhawech-Fauceglia P, Beck A, Miller A, Tsuji T, et al. Tumor-infiltrating NY-ESO-1-specific $CD8^+$ T cells are negatively regulated by LAG-3 and PD-1 in human ovarian cancer. *Proc Natl Acad Sci U S A* 2010;**107**:7875−80.
33. Sliwkowski MX, Mellman I. Antibody therapeutics in cancer. *Science* 2013;**341**:1192−8.
34. Wieder T, Eigentler T, Brenner E, Rocken M. Immune checkpoint blockade therapy. *J Allergy Clin Immunol* 2018;**142**:1403−14.
35. Fosgerau K, Hoffmann T. Peptide therapeutics: current status and future directions. *Drug Discov Today* 2015;**20**:122−8.
36. Weinmann H. Cancer immunotherapy: selected targets and small-molecule modulators. *ChemMedChem* 2016;**11**:450−66.
37. Vlieghe P, Lisowski V, Martinez J, Khrestchatisky M. Synthetic therapeutic peptides: science and market. *Drug Discov Today* 2010;**15**:40−56.
38. Vladimer GI, Snijder B, Krall N, Bigenzahn JW, Huber KVM, Lardeau CH, et al. Global survey of the immunomodulatory potential of common drugs. *Nat Chem Biol* 2017;**13**:681−90.
39. Zhang X, Wang F, Shen Q, Xie C, Liu Y, Pan J, et al. Structure reconstruction of LyP-1: ^{L}c(LyP-1) coupling by amide bond inspires the brain metastatic tumor targeted drug delivery. *Mol Pharm* 2018;**15**:430−6.
40. Magiera-Mularz K, Skalniak L, Zak KM, Musielak B, Rudzinska-Szostak E, Berlicki L, et al. Bioactive macrocyclic inhibitors of the PD-1/PD-L1 immune checkpoint. *Angew Chem Int Ed Engl* 2017;**56**:13732−5.
41. Molek P, Strukelj B, Bratkovic T. Peptide phage display as a tool for drug discovery: targeting membrane receptors. *Molecules* 2011;**16**:857−87.
42. Jerabek-Willemsen M, André T, Wanner R, Roth HM, Duhr S, Baaske P, et al. MicroScale thermophoresis: interaction analysis and beyond. *J Mol Struct* 2014;**1077**:101−13.
43. Hmama Z, Gabathuler R, Jefferies WA, Jong Gd, Reiner NE. Attenuation of HLA-DR expression by mononuclear phagocytes infected with *Mycobacterium tuberculosis* is related to intracellular sequestration of immature class II heterodimers. *J Immunol* 1998;**161**:4882−93.

44. He Y, Rivard CJ, Rozeboom L, Yu H, Ellison K, Kowalewski A, et al. Lymphocyte-activation gene-3, an important immune checkpoint in cancer. *Cancer Sci* 2016;**107**:1193−7.
45. Ascierto PA, Melero I, Bhatia S, Bono P, Sanborn RE, Lipson EJ, et al. Initial efficacy of anti-lymphocyte activation gene-3 (anti-LAG-3; BMS-986016) in combination with nivolumab (nivo) in pts with melanoma (MEL) previously treated with anti−PD-1/PD-L1 therapy. *J Clin Oncol* 2017;**35**:9520.
46. Tumeh PC, Harview CL, Yearley JH, Shintaku IP, Taylor EJ, Robert L, et al. PD-1 blockade induces responses by inhibiting adaptive immune resistance. *Nature* 2014;**515**:568−71.
47. Zhao M, Guo W, Wu Y, Yang C, Zhong L, Deng G, et al. SHP2 inhibition triggers anti-tumor immunity and synergizes with PD-1 blockade. *Acta Pharm Sin B* 2019;**9**:304−15.
48. Cook KD, Whitmire JK. LAG-3 confers a competitive disadvantage upon antiviral $CD8^+$ T cell responses. *J Immunol* 2016;**197**:119−27.
49. Scala E, Carbonari M, Porto PD, Cibati M, Tedesco T, Mazzone AM, et al. Lymphocyte activation gene-3 (LAG-3) expression and IFN-γ production are variably coregulated in different human T lymphocyte subpopulations. *J Immunol* 1998;**161**:489−93.
50. Giraldo NA, Becht E, Pages F, Skliris G, Verkarre V, Vano Y, et al. Orchestration and prognostic significance of immune checkpoints in the microenvironment of primary and metastatic renal cell cancer. *Clin Cancer Res* 2015;**21**:3031−40.
51. Durham NM, Nirschl CJ, Jackson CM, Elias J, Kochel CM, Anders RA, et al. Lymphocyte activation gene 3 (LAG-3) modulates the ability of CD4 T-cells to be suppressed *in vivo*. *PLoS One* 2014;**9**:e109080.
52. Farsam V, Hassan ZM, Zavaran-Hosseini A, Noori S, Mahdavi M, Ranjbar M. Antitumor and immunomodulatory properties of artemether and its ability to reduce $CD4^+$ $CD25^+$ $FOXP3^+$ Treg cells *in vivo*. *Int Immunopharmacol* 2011;**11**:1802−8.
53. Betts G, Jones E, Junaid S, El-Shanawany T, Scurr M, Mizen P, et al. Suppression of tumour-specific $CD4^+$ T cells by regulatory T cells is associated with progression of human colorectal cancer. *Gut* 2012;**61**:1163−71.
54. Gagliani N, Magnani CF, Huber S, Gianolini ME, Pala M, Licona-Limon P, et al. Coexpression of CD49b and LAG-3 identifies human and mouse T regulatory type 1 cells. *Nat Med* 2013;**19**:739−46.